ARTICLE

Design of Nickel Donor-Acceptor Dithiolenes for 2nd order Nonlinear Optics. Experimental and Computational study

iòReceived 00th January 20xx,
Accepted 00th January 20xx

DOI: 10.1039/x0xx00000x

Salahuddin. S. Attar,[a] Luciano Marchiò,*[b] Luca Pilia,*[c] Maria F. Casula,[c] Davide Espa,[d] Angela Serpe,[e] Maddalena Pizzotti[f] , Daniele Marinotto [g] and Paola Deplano*[d]

Structures and properties, including second-order non-linear optical properties in solution and in polymethylmethacrylate (PMMA) films, of new nickel heteroleptic Donor-Acceptor dithiolene complexes are reported here ([Ni(Bn$_2$pipdt)**L1**-**4**], **1**-**4**). The acceptor dithione system (Bn$_2$pipdt = 1,4-dibenzylpiperazine-2,3-dithione) is invariant, whereas the donor dithiolate moiety varies in **1** to **4** (i-mnt = 2,2-dicyanoethylene-1,1-dithiolate (**L1**), sqdt = 1,2-dithiosquarate (**L2**), ddmedt = 1,2-dicarbomethoxyethylene dithiolate (**L3**), dddmedt = 5,6-bis(methoxycarbonyl)-1,4dithiine-2,3-bis(thiolate) (**L4**). Molecular structural characterization of **1**, **3** and **4** points out that the metal center exhibits a square-planar geometry bound by the dithione ligand Bz$_2$pipdt, and by three different dithiolate-type ligands. Complexes **1**-**4** are characterized in the visible region by a peak of moderately strong intensity, which undergoes negative solvatochromism. The molecular quadratic optical nonlinearities were determined in DMF solution by the Electric Field Induced Second Harmonic generation technique, working with a 1907 nm incident wavelength. The $\mu\beta_{1907}$ values (−680 (**1**), −855 (**2**), −1080 (**3**); −1180 (**4**)) (10^{-48} esu) were measured, showing that **1**-**4** exhibit negative second-order polarizabilities whose values depend on the donor ligand. While **1**-**4** exhibit similar thermolytic behavior, when embedded into PMMA poled matrix, only **3** maintains second order NLO properties in the solid state. A good NLO response with a value of the three nonzero coefficients of the second-order susceptibility tensor $\chi_{33}^{(2)}$, $\chi_{31}^{(2)}$, and $\chi_{15}^{(2)}$ = 2.20 ± 0.44 pm V^{-1}, 0.56 ± 0.12 pm V^{-1} and 0.42 ± 0.08 pm V^{-1}, respectively, was found. According to computational studies the $\mu\beta_{1907}$ sequence is mainly related to the donor capability of the dithiolate ligands, which affects the HOMO-LUMO energy gap (2.05 (**1**), 1.80 (**2**), 1.56 (**3**), 1.36 (**4**) eV), and it can thus modulate the position of the low-energy absorption and related properties in the series.

Introduction

The design of new compounds with large second order nonlinear optical (NLO) properties is of interest for both fundamental scientific purposes and also to provide molecular building blocks for advanced photonic materials.[1,2] Second-order NLO effects arise from the first hyperpolarizability β, which at the molecular level relates to the way in which the mobile electronic charges respond to the oscillating electric field of a laser beam. Large values of this parameter typically occur in non-centrosymmetric, π-bridged molecules with electron donor and acceptor substituents. In addition, a polar ordering of the NLO chromophore is required to observe bulk quadratic NLO effects. Molecules with extensive π-delocalized system are suitable to promote such properties related to the polarizability of the electrons and dependent on electronic transitions with high charge transfer (CT) character.

Organic compounds containing electron-donor and electron-acceptor groups connected by a π-bridge and giving rise to an asymmetric charge distribution in the ground state have been and still are extensively investigated as suitable 2nd NLO-phores. Transition metal complexes, where the metal acts as a coordinating bridge between the Donor and Acceptor ligands have progressively increased their role in this field, because, in addition to improved stability for ligands, the metal can favour co-planarity through its preferred coordination geometry, maximizing the CT Donor-Acceptor transition. Moreover, a proper design allows to select ligands whose frontiers orbitals energies fall between filled and empty d-orbitals. Thus, CT transitions may be tunable by virtue of the nature, oxidation state, and coordination sphere of the metal centre, while the

[a] *Texas A&M University at Qatar (TAMUQ) Texas A&M Engineering Building, Education City, Doha (Qatar).*
[b] *Dipartimento di Scienze Chimiche, della Vita e della Sostenibilità Ambientale, Università di Parma, Parco Area delle Scienze 11/a, 43124, Parma (Italy).*
[c] *Dipartimento di Ingegneria Meccanica, Chimica e dei Materiali, Università di Cagliari, Via Marengo 2, 09123, Cagliari (Italy).*
[d] *Dipartimento di Fisica, INSTM Research Unit, Università di Cagliari, 09042, Monserrato (CA) (Italy).*
[e] *Dipartimento di Ingegneria Civile, Ambientale e Architettura, Università di Cagliari, Via Marengo 2, 09123, Cagliari (Italy).*
[f] *Department of Chemistry, INSTM Research Unit, University of Milan, Via C. Golgi 19, 20133 Milano (Italy).*
[g] *ISTM-CNR, Via C. Golgi 19, 20133 Milano (Italy), Centro CIMAINA dell'Università degli Studi di Milano e UdR dell'INSTM*

Electronic Supplementary Information (ESI) available: Crystal packing of **1**, **3**·**DMF** and **4**·**DMF** (Figure S1); simulated UV-Vis spectra (Figure S2-S6); tables containing TD-DFT calculated electronic transitions (Tables S1-S4); molecular orbitals and corresponding energies for complexes **1**-**4** (Figure S7); details on spin-coating depositions (Table S5); poling of complexes **1**, **2** and **4** (Figures S8-S10); details on SHG measurements. "This material is available free of charge via the Internet at http://pubs.acs.org."

advantages of the versatility of organic ligands, which can be properly engineered to favour the incorporation of the molecules into suitable polymeric matrices, are maintained.[3-5] Square-planar heteroleptic d^8-metal–dithiolene complexes, have been shown to work as tunable second-order NLO chromophores.[6-11] The requirement to obtain this property is achieved with the presence of two ligands occurring in formally different oxidation states, one reducing (dianionic = dithiolate, electron Donor = D), and the other oxidizing (neutral = dithione or diimine, electron Acceptor = A), with the metal (M) acting as a π-bridge. These noncentrosymmetric molecules (D-M-A), exhibit an absorption peak in the visible spectral region, which is tunable with the HOMO–LUMO energy gap. Specifically, the donor gives a prevailing contribution to the HOMO, and the acceptor mainly contributes to the LUMO, and the coordinated metal provides the bridge for the electron transfer. Accordingly, the charge transfer (CT) Donor–Acceptor process produces a decrease of the dipole moment from the ground to the excited state and, as a consequence, negative solvatochromism and first hyperpolarizability (β) are observed. Thus, the CT in these systems controls both the linear and the nonlinear optical properties and can be readily modulated by a proper selection of the ligands, and by chemical (protonation) or electrochemical stimuli.[12, 13]

However, these non-centrosymmetric complexes present a dipolar moment in the ground state which favors a centrosymmetric arrangement of these molecules in the crystal lattice, leading to a loss of the second-order NLO property in the bulk. To overcome this drawback, NLO chromophores are embedded into polymeric poled films.[11,14,42] To obtain a sufficiently stable second-harmonic generation (SHG) signal of thin films, chromophores are required to possess suitable properties (good solubility, thermal stability, no aggregation for stacking) to be incorporated homogeneously in the host matrix of poled film and remain so within the time. To meet these requirements, we are investigating square-planar heteroleptic d^8-metal–dithiolene[6,12-15] characterized by remarkable high negative molecular first hyperpolarizability both at the molecular level and in the bulk. With the view to find processable candidates, we have designed and prepared the complexes shown in Chart 1, which share the same acceptor ligand Bn_2pipdt (1,4-dibenzylpiperazine-2,3-dithione) but differ for the dithiolato ligand. Compound **1** bears the 1,1-dithiolato= i-mnt as donor ligand, in **2** the donor 1,2-dithiolato presents CO as part of a rigid and planar system. On the other hand, conformationally flexible ester groups are present in **3**, and **4**. Furthermore, in **4** the ester groups are at a longer distance from the dithiolato moiety and with linkers consisting of S-atoms inserted in a hexa-atomic ring. These terminal groups have been introduced to improve both the hydrophilic character and the solubility in various solvents of the NLO-phores and to limit their aggregation once included into the polymeric film.

Specifically, the nature of the donor ligand can have influence on the following aspects: a) on second order NLO response[14]; b) in the thermal stability of the compounds; c) in promoting

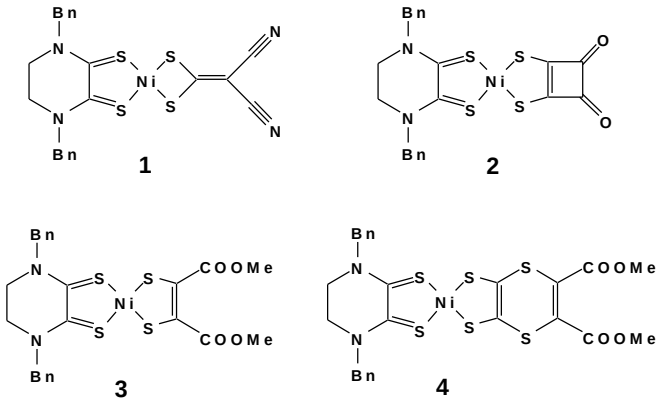

Chart 1

the incorporation of the complexes into a PMMA poled matrix, thus providing a good and stable NLO response in the bulk.

The molecular structure of the complexes are reported, together with a computational study by means of density functional theory (DFT) allowed rationalizing the observed properties.

Experimental

Materials and methods. Reagents and solvents were purchased from Aldrich and used without further purification. IR spectra (4000–400 cm^{-1}) were recorded with a Bruker Tensor 27 Platinum ATR. Electronic absorption spectra were recorded with an Agilent Cary 5000 spectrophotometer.

Complexes preparation. Complex [Ni(Bn_2pipdt)Cl_2] and ligands $\mathbf{L_1}$-$\mathbf{L_4}$ were prepared according to references 12, 16, 17, 18, and 19.

[Ni(Bn_2pipdt)(i-mnt)] (**1**) [Ni(Bn_2pipdt)Cl_2] (80.0 mg, 0.175 mmol) dissolved in 15 mL of methanol (green solution) was added drop-wise to a dark red solution of Na_2(i-mnt) (32.6 mg, 0.175 mmol) in 25 mL methanol. The mixture was stirred and refluxed and after 24 hours a green microcrystalline solid was formed (79.6 mg; yield: 86.4%). This solid was filtered, washed with diethyl ether and then dried. Analytical results are in accordance with the formula [Ni(Bn_2pipdt)(i-mnt)]. Elemental Analysis: calculated for C22H18N4NiS4 (525.36): C, 50.30; H, 3.45; N, 10.66; S, 24.41; found: C, 50.7; H, 3.4; N, 10.7; S, 24.5; UV-Vis-NIR (DMF solution): λ (nm) ε ($M^{-1}cm^{-1}$): 257 (1.52×10^4); 327 (4.7×10^4); 350sh; 582sh; 678 (6.52×10^3); FT–IR (KBr): ν_{max} (cm^{-1}): 3031 (vw); 2867 (w); 2195 (s) ($\nu CN_{i\text{-}mnt}$); 1533 (s) (νCN_{pipdt}); 1428 (s) (νCC); 1398 (s); 1375 (s); 1361 (s); 1259 (w); 1184 (m); 1110 (w); 1029 (vw); 939 (w); 893 (w); 738 (m); 698 (m), 604 (vw); 547 (w); 476 (w). Well-formed crystals suitable for X-ray crystallography were obtained through re-crystallization from DMF/diethyl ether, corresponding to [Ni(Bn_2pipdt)(i-mnt)].

[Ni(Bn_2pipdt)(sqdt)] (**2**) This complex was prepared by following the same procedure reported for **1** using 100.0 mg (0.219 mmol) of [Ni(Bn_2pipdt)Cl_2] in 25 mL of methanol and 43.5 mg (0.219 mmol) of Na_2(sqdt) in 25 mL of the same solvent (95.8 mg of **2**; yield: 82.6%). Analytical results are in

accordance with the formula [Ni(Bn$_2$pipdt)(sqdt)]. Elemental Analysis: calculated for C22H18N2NiO2S4 (529.34): C, 49.92; H, 3.43; N, 5.29; S, 24.23; found: C, 50.0; H, 3.4; N, 5.3; S, 24.3; UV-Vis-NIR (DMF solution): λ (nm) ε ($M^{-1}cm^{-1}$): 259 (2.76×10^4); 319 (4.64×10^4); 635sh; 737 (7.44×10^3); FT–IR (KBr): ν_{max} (cm^{-1}): 3032 (vw); 2927 (w); 1817 (vw); 1742 (vs) (νCO); 1705 (s); 1652 (m); 1524 (s) (νCN); 1428 (s) (νCC); 1359 (s); 1256 (m); 1160 (m); 1113 (w); 937 (vw); 875 (vw);739 (m); 698 (m); 668 (vw) 525 (w).

[Ni(Bn$_2$pipdt)(ddmedt)] (**3**) This compound was synthesized by following a modified procedure reported for **1** using 100.0 mg (0.219 mmol) of [Ni(Bn$_2$pipdt)Cl$_2$] in 25 mL of methanol and 52.2 mg (0.219 mmol) of Na$_2$(ddmedt) in 25 mL of the same solvent (101.6 mg; yield: 78.4%). The solution of Na$_2$(ddmedt) was prepared adding the compound 4,5-bis(methyloxycarbonyl)-1,3-dithiole-2-one to a sodium methoxide solution. Analytical results are in accordance with the formula [Ni(Bn$_2$pipdt)(ddmedt)]. Elemental Analysis: calculated for C24H24N2NiO4S4 (591.41): C, 48.74; H, 4.09; N, 4.74; S, 21.69; found: C, 48.8; H, 4.2; N, 4.8; S, 21.7; UV-Vis-NIR (DMF solution): λ (nm) ε ($M^{-1}cm^{-1}$): 262 (1.28×10^4); 314 (1.97 ×10^4); 830 (6.06 ×103); FT–IR (KBr): ν_{max} (cm^{-1}): 3060 (vw); 2962 (m); 2954 (w); 1714 (s)(νCO); 1557 (s); 1520 (m)(νCN); 1453 (w); 1432 (m) (νCC); 1357 (m); 1234 (vs); 1118 (vw); 1081 (w); 1028 (m); 766 (vw);738 (w); 695 (w); 667 (vw); 620 (vw). Crystals suitable for X-ray crystallography were obtained through re-crystallization from DMF/diethyl ether, corresponding to [Ni(Bn$_2$pipdt)(ddmedt)]·DMF.

[Ni(Bn$_2$pipdt)(dddmedt)] (**4**) Complex **4** was synthesized in accordance to a modified method reported above for **1** using 80.0 mg (0.175 mmol) of [Ni(Bn$_2$pipdt)Cl$_2$] in 25 mL of methanol and 59.6 mg (0.175 mmol) of Na$_2$(dddmedt) in 25 mL of the same solvent (107.2 mg; yield: 90.1%). The solution of Na$_2$(dddmedt) was prepared adding the corresponding 1,3-dithiole-2-one compound to a sodium methoxide solution.

Analytical results are in accordance with the formula [Ni(Bn$_2$pipdt)(dddmedt)]. Elemental Analysis: calculated for C26H24N2NiO4S6 (679.56): C, 45.95; H, 3.56; N, 4.12; S, 28.31; found: C, 45.8; H, 3.5; N, 4.2; S, 28.4; UV-Vis-NIR (DMF solution): λ (nm) ε ($M^{-1}cm^{-1}$): 262 (1.12×10^4); 321 (2.97×10^4); 872 (7.96×10^3); FT–IR (KBr): ν_{max} (cm^{-1}): 3030 (vw); 2950 (w); 2917 (vw); 1729 (s) (νCO); 1566 (m); 1516 (s)(νCN); 1431(m) (νCC); 1357(s); 1249 (vs); 1074 (m); 1110 (m); 899 (vw); 737 (m); 698 (w); 460 (vw). Crystals suitable for X-ray crystallography were obtained through re-crystallization from DMF/diethyl ether, corresponding to [Ni(Bn$_2$pipdt)(dddmedt)]·DMF.

Computational Details. The electronic properties of the [Ni(Bn$_2$pipdt)(L$_N$)] complexes (L$_N$ = **L$_1$**–**L$_4$** = dithiolate ligand) were investigated by means of DFT methods using the spin unrestricted formalism.[20] All the calculations were performed with the Gaussian 16 program suite.[21] The molecular structures of **1**-**4** complexes were optimized starting from the X-ray experimental geometry for **1**, **3** and **4**, and by a suitable molecular model for **2**. The Becke three-parameters exchange functional with Lee-Yang-Parr correlation functional (B3LYP)[22,23] was employed together with the 6-31+G(d) basis set[24,25] for the C, H, N, and S atoms, the Ni atom was treated with the SDD valence basis set[26,27] and with the MDF10 effective core potentials. Single point calculations were performed at the same level of theory of the geometry optimizations. Molecular orbital diagrams were generated with the *ArgusLab* program.[28] The electronic structure was analyzed using the *AOMix* program.[29,30]

X-ray crystallography. A summary of data collection and structure refinement for **1**, **3** and **4** is reported in Table 1. Single crystal data were collected with a *Bruker Smart Breeze* area detector diffractometer, Mo Kα: λ = 0.71073 Å (**1**), and at the X-ray diffraction beamline (XRD1) of the Elettra Synchrotron, Trieste (Italy) (**3** and **4**) using a monochromatic wavelength of 0.700 Å on a Pilatus 2M hybrid-pixel area detector. For **1**, the intensity data were integrated from several series of exposures frames (0.3° width) covering the sphere of reciprocal space,[31] and an absorption correction was applied using the program SADABS[32]. For **3** and **4**, complete datasets were collected at 100 K (nitrogen stream supplied through an Oxford Cryostream 700) through the rotating crystal method. For **3**, complete datasets were obtained merging two different data collections done on the same crystal, mounted with different orientations. The diffraction data were then indexed and integrated using XDS.[33] All the structures were solved with ShelxT[34] and refined on F^2 with full-matrix least squares (ShelxL[35]), using the Olex2 software package.[36] Non-hydrogen atoms were refined anisotropically and the hydrogen atoms were placed at their calculated positions. Graphical material was prepared with the Mercury 3.10[37] program. CCDC 1910384-1910386 contain the supplementary crystallographic data for this paper.

Thermogravimetric analysis. Thermogravimetric analysis (TGA) were performed on a SDT Q600 DSC-TGA analyzer under N_2 atmosphere (gas flow 50 mL·min^{-1}). The samples were placed into an alumina pan and submitted to a thermal treatment as follows: isothermal at room temperature for 3 minutes; heating at a ramp of 10 °C·min^{-1} up to 1200 °C, and kept at the final temperature for 5.00 min.

Second-order Nonlinear Optical Properties. The second order NLO responses of the molecular chromophore was measured by the EFISH (Electric Field Induced Second Harmonic generation) technique, which provides the γ_{EFISH} value, from which EFISH quadratic hyperpolarizability β_λ can be obtained through eq. 1

$$\boldsymbol{\gamma_{EFISH} = (\mu\beta_\lambda/5kT) + \gamma(-2\omega;\omega,\omega,0)} \quad (1)$$

where μ is the ground state dipole moment, $\mu\beta_\lambda$/5kT the dipolar orientational contribution, λ is the fundamental wavelength of the incident photons in the EFISH experiment, γ(-2ω; ω,ω,0) is a third-order term at frequency ω of the incident photons, corresponding to the cubic contribution to γ_{EFISH}, usually negligible for dipolar chromophores such as those studied in this work. Finally, β_λ is the projection along the dipole moment axis of the vectorial component β_{VEC} of the tensorial quadratic hyperpolarizability. In the following, β_λ is reported as β_{1907} since the EFISH experiments were carried out

working with a 1907 nm incident wavelength. All the EFISH measurements were carried out in DMF solutions at 10^{-3} M concentration and the experimental $\mu\beta_{1907}$ values obtained are the averages of 16 measurements. All experimental EFISH $\mu\beta_{1907}$ values are defined according to the "phenomenological" convention.[38]

Polymer film: preparation and characterization. Composite thin films of **1**, **2**, **3** and **4** in poly(methyl methacrylate) (PMMA, $\bar{M}_w$ ~ 15000; T_g = 86.5 °C as determined by differential scanning calorimetry) were deposited by spin-coating (Cookson Electronic Company P-6708D Spin-coater, spinning parameters: RPM1 = 800; ramp2 = 1 s; time1 = 5 s; RPM2 = 2000; ramp2 = 1 s; time2 = 60 s) on glass slide substrate. Solutions were prepared in CH_3CN keeping 5 wt% of **1**, **2**, **3** and **4** complexes with respect to PMMA (see Table S5). The thickness of **1**, **2**, **3** and **4** films was measured by α-step stylus profilometer (Bruker DektakXT) to be 1.15 ± 0.07 µm, 1.8 ± 0.11 µm, 2.21 ± 0.13 µm and 1.16 ± 0.07µm, respectively.

Corona-wire Poling Setup. The fundamental incident light was generated by a 1064 nm Q-switched Nd:YAG (Quanta System Giant G790−20) laser with a pulse of 7 ns and 20 Hz repetition rate. The output pulse was attenuated to 0.50 mJ and focused with a lens (f = 600 mm) on the sample, placed over the hot stage. Corona poling process was performed inside a drybox under N_2 atmosphere. The fundamental beam was polarized in the incidence plane (so-called p-polarized) with an angle of about 55° with respect to the sample in order to optimize the SHG signal. The hot-stage temperature was controlled by a GEFRAN 800 controller, while the corona-wire voltage (up to 9.5 kV across a 10 mm gap) was applied by a TREK 610E high voltage supply. After rejection of the fundamental beam by an interference filter and a glass cut-off filter, the p-polarized SHG signal at 532 nm was detected with a UV−vis photomultiplier (PT, Hamamatsu C3830). The output signal from the PT was set to a digital store oscilloscope and then processed by a computer with dedicated software.

Maker fringe measurement. In the Maker fringe experiment, the second harmonic intensity was detected as a function of the incidence angle θ of the fundamental beam and normalized with respect to that of a calibrated quartz crystal wafer (X-cut) 1 mm thick whose d_{11} is 0.46 pmV^{-1}. In order to determine the nonzero independent components of the susceptibility tensor ($\chi_{ij}^{(2)}$) for poled films ($C_{\infty v}$ symmetry), Maker fringe measurements were conducted with different polarizations of the fundamental and SH beam: p → p, s → p, and 45° → s (where p and s indicate the polarization of the beam in the plane parallel and orthogonal to the incident one, respectively).[39-41]

Table 1. Crystal data and structure refinement for **1**, **3·DMF** and **4·DMF**.

	1	**3·DMF**	**4·DMF**
Empirical formula	$C_{22}H_{18}N_4S_4Ni$	$C_{27}H_{31}N_3NiO_5S_4$	$C_{29}H_{31}N_3NiO_5S_6$
Formula weight	525.35	664.50	752.64
Temperature/K	296	100.0	100
Crystal system	triclinic	triclinic	monoclinic
Space group	P-1	P-1	$P2_1/n$
a/Å	9.040(3)	10.3749(3)	17.6638(2)
b/Å	11.556(3)	12.0393(5)	8.31590(10)
c/Å	12.136(4)	13.1825(5)	23.1526(2)
α/°	73.582(4)	64.188(4)	90
β/°	70.444(5)	89.513(3)	108.2360(10)
γ/°	83.313(5)	81.625(3)	90
Volume/$Å^3$	1145.6(6)	1463.70(10)	3230.09(6)
Z	2	2	4
$\rho_{calc}g/cm^3$	1.523	1.508	1.548
μ/mm^{-1}	1.229	0.952	0.993
F(000)	540.0	692.0	1560.0
Crystal size/mm^3	0.29 × 0.19 × 0.15	0.11 × 0.07 × 0.07	0.11 × 0.09 × 0.08
Radiation	MoKα (0.71073 Å)	synchrotron (0.700 Å)	synchrotron (0.700 Å)
2Θ data collection/°	3.676 to 49.65	3.386 to 51.884	3.432 to 49.246
Refl. Collec./Indep.	12122/3935 [R_{int} = 0.0348]	22675/5910 [R_{int} = 0.0455]	16441/5438 [R_{int} = 0.0241]
Data/restraints/param.	3935/6/299	5910/0/366	5438/0/401
Goodness-of-fit on F^2	1.004	1.041	1.093
R_1 [I>=2σ (I)]	0.0323	0.0308	0.0347
wR_2 [I>=2σ (I)]	0.0825	0.0788	0.1197

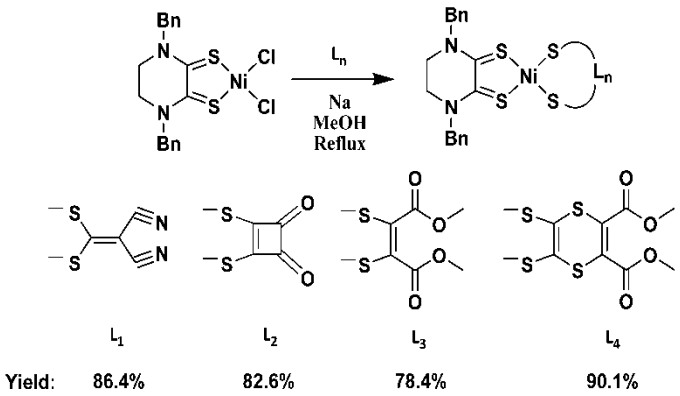

Scheme 1

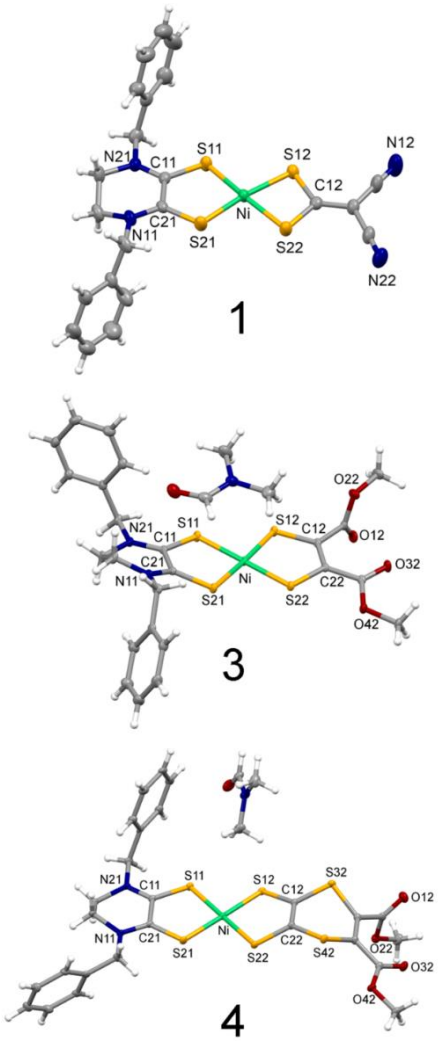

Figure 1. Molecular structure of [Ni(Bn_2pipdt)(i-mnt)] (**1**), [Ni(Bn_2pipdt)(ddmedt)] ·DMF (**3·DMF**) and [Ni(Bn_2pipdt)(dddmedt)]·DMF (**4·DMF**) with thermal ellipsoids drawn at the 30% probability level.

Results and discussion

Chart 1 and Scheme 1 show the chemical structures and synthetic approach for the series of heteroleptic nickel-dithiolene complexes **1-4**. As anticipated in the Introduction, these complexes were designed to have the same acceptor ligand Bn_2pipdt (1,4-dibenzylpiperazine-2,3-dithione) but to differ for the dithiolato ligand, having electrodonating properties increasing from **1** to **4**, in agreement with the nature of substituents in **L1**-**L4**. In particular, L**1** (i-mnt) contains CN substituents conjugated to a 1,1-dithiolate anion, namely 2,2-dicyanoethylene-1,1-dithiolate. **L1** is analogous, but electronically different, to the 1,2 dithiolate system (mnt). As far as the other anions are concerned, all have carbonyl groups, which are constrained in co-planarity in **L2**, whereas in **L3** and **L4** the ester groups are directly attached at the dithiolate moiety, or through a sulphurated linker, respectively. All these chromophores exhibit good solubility in common organic solvents. Crystals suitable for X-ray diffractometric characterization were obtained for complexes **1**, **3** and **4**, and related results are described below.

Structural Descriptions of Complexes 1, 3 and 4.

The X-ray molecular structures of compounds **1**, **3** and **4** are reported in Figure 1. All compounds exhibit the metal center in a square-planar geometry bound by the dithione ligand Bn_2pipdt, and by three different dithiolate-type ligands, i-mnt, ddmedt and dddmedt. In Table 2 are reported the comparisons of the experimental and optimized molecular geometries, which show a good agreement. More specifically, and elaborating on the bond distances, it is evident that the two thione functions of Bn_2pipdt are connected by a single C-C bond (C11-C21), whereas the dithiolate system in **3**-**4** are connected by a partial double bond between the carbon atoms (C12-C22). These geometric features are in agreement with previously reported structures of d^8 metal square-planar heteroleptic dithiolenes, where one of the ligands acts as dithione, the other as dithiolate.[12,14,15,42-47] By inspecting the Ni-S bond lengths it appears that there is not a trend in the distances distribution for the three reported experimental geometries. A clearer situation occurs for the C-S bond lengths, since those of the Bn_2pipdt ligand are significantly shorter than those of the i-mnt, ddmedt and dddmedt ligands, in support of the formulation of Bn_2pipdt as a dithione and i-mnt, ddmedt and dddmedt as dithiolate systems.

Thermal stability

In view of potential applications, the second order NLO chromophores must withstand processing conditions required for dispersion into suitable matrices, such as polymerization or glass formation temperatures. Thermal stability of the chromophores was assessed by thermogravimetric analysis, which is reported in Figure 2, indicating that the samples exhibit a relatively similar thermolytic behaviour. All the samples exhibit a negligible weight loss until 200 °C, suggesting

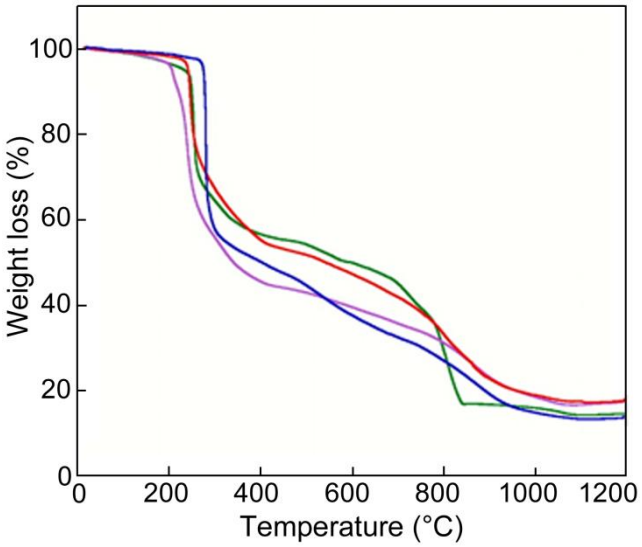

Figure 2. Thermogravimetric curves of [Ni(Bn_2pipdt)(i-mnt)] (**1**) (blue), [Ni(Bn_2pipdt)(sqdt)] (**2**) (red), [Ni(Bn2pipdt)(ddmedt)] (**3**) (green) and [Ni(Bn_2pipdt)(dddmedt)] (**4**) (purple).

therefore, their stability up to this temperature. In the range 210- 280 °C a sharp weight loss (around 40%) is observed, followed by a smoother weight loss. Complete degradation is observed at temperatures in the range 840-940°C, leading to a final mass in the range 13-17 wt% which is consistent with the formation of nickel sulphide. These data indicate that the selected substituents lead to nickel complexes with suitable thermal stability as required for operating conditions and further materials processing.

Optical properties and DFT calculations

In the visible region, DMF solutions of **1**–**4** are characterized by a broad peak with a more or less resolved shoulders-peaks at higher frequency, as shown in Figure 3 and reported in Table 3. The peaks at lower frequency show negative solvatochromic behaviour, as reported in Figure 4 for **4** as an example. These findings are in accordance with what previously observed by us in this class of compounds describable as D-M-A molecules, where the CT Donor–Acceptor process produces a decrease of the dipole moment from the ground to the excited state and, as a consequence, negative solvatochromism.

With the aim to shed light on the electronic transitions, TD-DFT calculations were performed both in gas-phase and DMF. The simulated spectra (Figure S2-S6) reproduce quite well the experimental ones. Moreover, the low-energy absorption is almost entirely associated to the HOMO-LUMO transition in **3** and **4 (**see Tables S1-S4) while it is heavily dependent on the HOMO-LUMO transition (>60%) and to a minor but significant extent to the HOMO-LUMO+1 transition (in **1** and **2**). These results show the considerable influence exerted by the dithiolate ligand in modulating the position of the low-energy absorption, and evidence also that the simplified two-state model proposed by Oudar can be applied only in compounds **3** and **4**, given that in **1** and **2** more than two states are

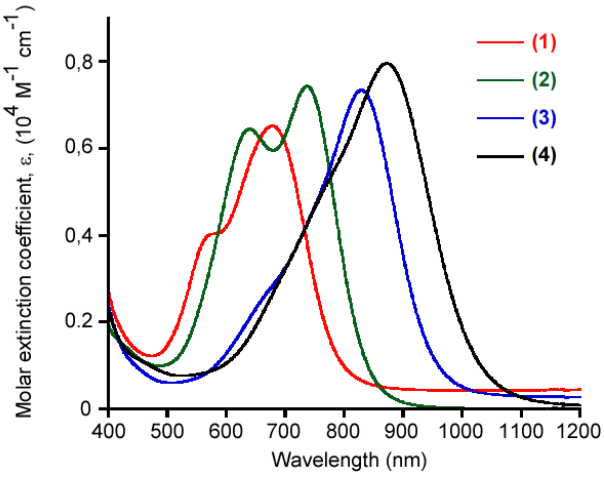

Figure 3. Electronic absorption spectra of **1**, **2**, **3** and **4** in DMF solutions (conc. = $1.0 \cdot 10^{-4}$ M).

associated to the low energy transition (Figure S6).

EFISH experiments, performed at 1907 nm and using DMF solutions, allowed to determine the scalar product $\mu\beta_\lambda$ (μ = ground state dipole moment; β_λ= projection of the vectorial component of the quadratic hyperpolarizability tensor along the dipole moment axis) with an uncertainty of about 10%.

These data, collected in Table 3, exhibit negative second order polarizability which, for chromophores 3 and 4, can be affected by some resonance enhancement because the second harmonic 2ω at 950 nm is quite close to the tail of λ_{max} (Figure 3).

Despite large values also observed for some platinum heteroleptic dithiolenes,[12] these compounds suffer from limited solubility in common organic solvents. This potential drawback, coupled with the high cost of the noble metal, makes **1-4** more appealing candidates to be investigated for embedding them in poled polymers.

In accordance with the negative solvatochromism, the $\mu\beta_\lambda$ values are negative. The sequence of energy of the CT band is

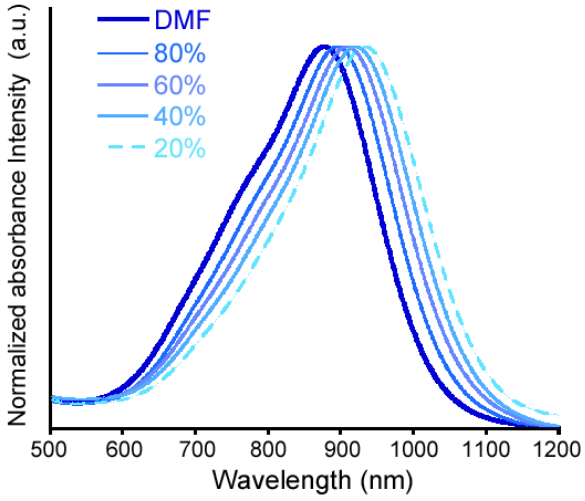

Figure 4. Electronic absorption spectra of **4** in DMF/CS_2 mixtures ranging from DMF 100% to 20% showing the negative solvatochromic behaviour.

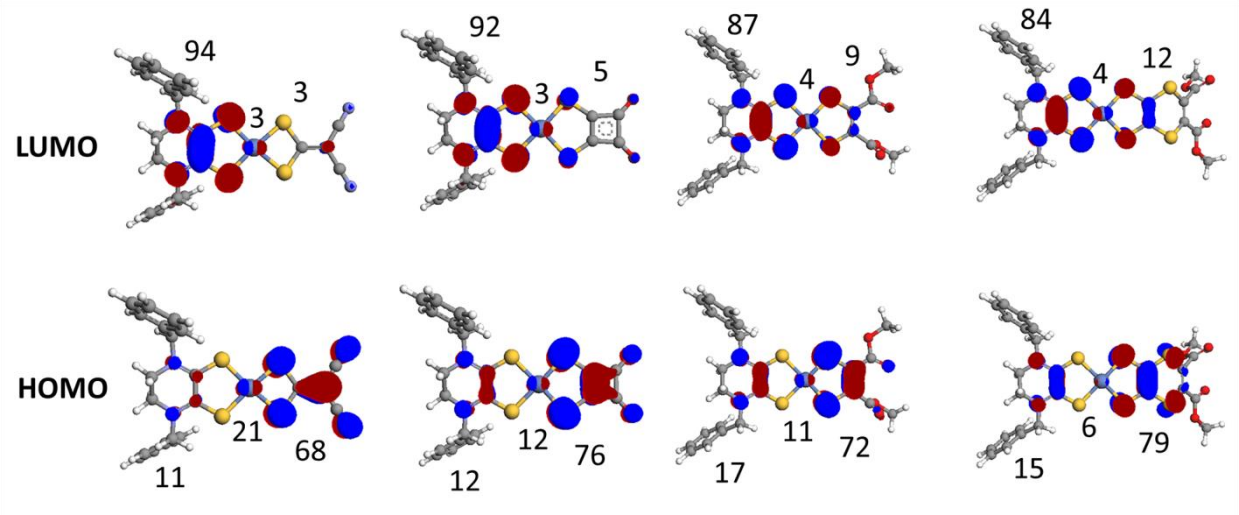

Figure 5. Fragmental composition (%) of the frontier molecular orbitals for **1**-**4**. The three fragments correspond to the metal centre and the two ligands, respectively.

associated to the HOMO-LUMO gap, in agreement with the presence of electron-withdrawing groups attached to the dithiolene moiety, which are expected to influence the energy of the HOMO orbitals. The frontier molecular orbitals (FOs) of the investigated compounds are shown in Figure 5 (and Figure S7) along with their fragmental compositions. As one can observe, as a general trend, the HOMOs are mainly formed by the orbitals of the donor ligand with contributions from the metal in antibonding interaction. This contribution ranging from 21 (**1**) to 6% (**4**), reflects a better matching in energies of metal orbital with donor ligand orbitals, according to the substituents electro-withdrawing influence (**1** > **2** > **3** > **4**), but these differences are not so high to affect significantly the expected HOMOs energies sequence.

As far as the LUMOs are concerned, the piperazinedithione ligand (the acceptor) is by far the main component of these FOs. These findings are in accordance with a CT character

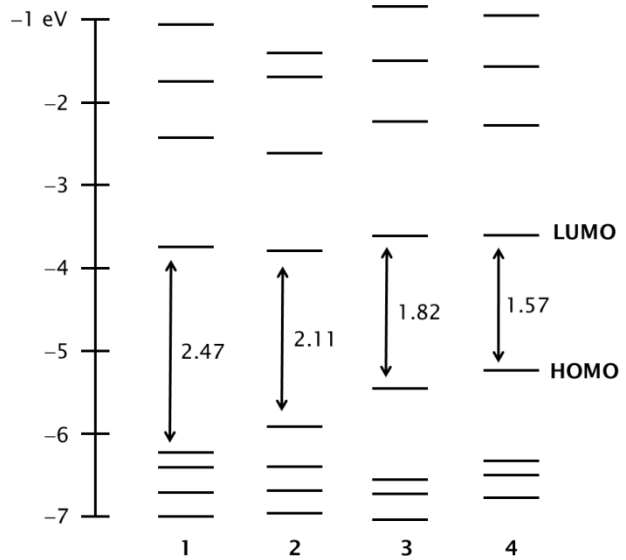

Figure 6. Frontier molecular orbital for **1-4**. Computational method PCM (DMF), B3LYP/6-31+G(d)-SDD.

associated to the HOMO-LUMO transition, which is, as mentioned above, a crucial feature for β generation. The energy gaps between the FOs decrease by 0.90 eV on going from complex **1** to **4**, in agreement with the experimentally observed trend in the HOMO-LUMO transition, which is, as mentioned above, a crucial feature for β generation. The energy gaps between the FOs decrease by 0.90 eV on going from complex **1** to **4**, in agreement with the experimentally observed trend in the absorption spectra (see Figure 6). As expected, and taking into account the FOs' compositions, these differences in the gaps are mainly due to the HOMO's energy level, which experiences a significant destabilization going from **1** to **4**, as a consequence the decreased electron-withdrawing capabilities from **L1** to **L4**.

The observed sequence of $\mu\beta_\lambda$ and of the inverse of the transition energy between the ground and excited state (ΔE_{ge}), the crucial factor to achieve high β regardless of the other factors, seems to be in agreement with the relationship proposed by Oudar: $\beta \propto (\mu_g - \mu_e)(\mu_{ge})^2/(\Delta E_{ge})^2$ (where μ_e and μ_g are the excited state and the ground state dipole moments; μ_{ge} is the transition state dipole moment) if a simplified two-state model can be applied.[48]

NLO properties of the PMMA films

The second-order NLO properties of the complexes **1**, **2**, **3** and **4** in the solid state, were measured working at 1064 nm incident wavelength and the thin films of the chromophores

Table 3. Optical and EFISH results for 1-4 complexes in DMF; the uncertainty of the EFISH measure is between ± 10 %.

Complex	λ_{max} (nm) [ε 10^4 (M^{-1} cm^{-1})]	μβλ (10^{-48}) esu
1	565 [3.9]; 678 [6.5]	−680
2	639 [6.4]; 737 [7.4]	−855
3	830 [6.1]	−1080
4	872 [8.0]	−1180

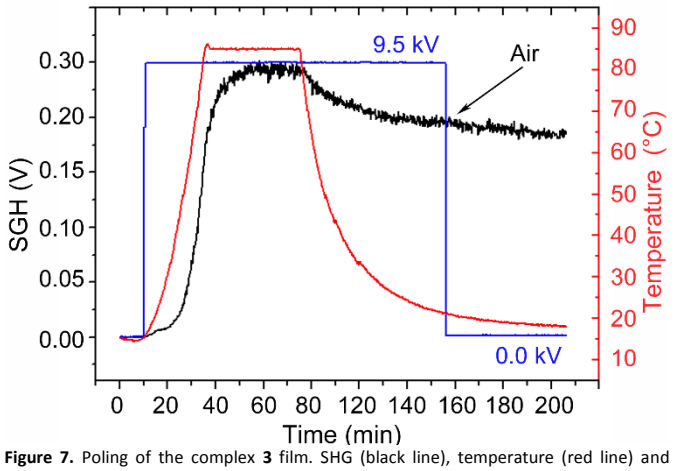

Figure 7. Poling of the complex **3** film. SHG (black line), temperature (red line) and electric field (blue line).

dispersed in a PMMA matrix were prepared as reported in the Experimental Section. Before poling, films were placed over the stage inside a drybox in which at least three cycles of vacuum-nitrogen were applied in order to keep the oxygen presence as low as possible.

The corona-wire poling dynamics of the chromophore **3** is shown in Figure 7 while those of **1, 2** and **4** are shown in Figures S8-S10, respectively.

For each sample, an optimization of the temperature and applied electric field during the poling is necessary both to avoid degradation of the film and to increase the SHG signal as much as possible. Analyzing the poling dynamics of the investigated 1, **2**, **3** and **4** films a general behavior can be observed. The SHG signal is negligible at room temperature and increases as the temperature is increased (around Tg of the PMMA) and the electric field is applied (9.5 kV), reaching its maximum value in about 30-40 min. This is due to the decrease of the viscosity of the polymeric matrix near to Tg which allowed an easier orientation of the NLO chromophores. After the SHG signal has reached the plateau, the temperature is decreased at room temperature, the drybox is opened and the electric field is turned off. However, during the cooling process, we observed a much faster decrease of the SHG signal for the films of **1**, **2** and **4** than for the film of **3**, presumably as a consequence of the reorientation of the chromophores within the polymeric matrix.[49] This phenomenon was explained by means of molecular dynamics simulations on various electric field poled organic NLO-phores.[50] After poling, the SHG signal of the films **1**, **2** and **4** were almost zero, and only the film **3** had a higher and stable SHG response; therefore, we will focus our attention on the film of the complex **3**.

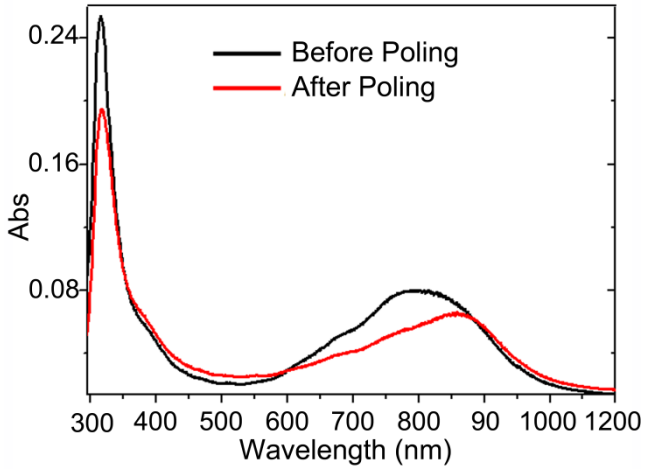

Figure 8. Electronic absorption spectra of the complex 3 film before and after poling.

Electronic absorption spectra on the film of the complex **3** before and after poling are reported in Figure 8. After poling, we note a decrease of the absorption bands (at peaks 316 and 804 nm) compared to those measured before poling (so-called dichroic effect) due to the partial orientation of molecules along the direction of the electric poling field.[51,52]

By fitting the Maker fringe measurements of the poled thin film of the complex **3,** using the expressions expected for poled film with $C_{\infty v}$ symmetry (see SI equations 1a–1c), the three nonzero coefficients of the second-order susceptibility tensor $\chi_{33}^{(2)}$, $\chi_{31}^{(2)}$, and $\chi_{15}^{(2)}$ are evaluated: 2.20 ± 0.44 pm V^{-1}, 0.56 ± 0.12 pm V^{-1} and 0.42 ± 0.08 pm V^{-1}, respectively. We consider Kleinman's symmetry ($\chi_{31}^{(2)} = \chi_{15}^{(2)}$) valid, as a very low absorption at the second harmonic (532 nm) is observed in the poled film, and we do not observe any absorption at the fundamental wavelength of 1064 nm (Figure 8). Moreover, although these values of the second-order susceptibility tensor are not very high, they are slightly better than those obtained for similar PdII dithione/dithiolate metal complex NLO-phores in PMMA matrix ($X_{33}^{(2)}$= 1.86 pmV^{-1}, $X_{31}^{(2)}$= 0.24 pmV^{-1}, $X_{15}^{(2)}$= 0.20 pmV^{-1}).[14] These results foster to further investigate[53] the use of Ni-complexes in alternative to Pd- or Pt-ones, given the Ni higher earth abundance and lower cost production.

The reason of the different behaviour for the films of **1**, **2**, **4** and **3** is not clear. Given the samples **1**-**4** exhibit a relatively similar thermolytic behaviour, the loss of SHG signal for the **1**, **2** and **4** films, is not ascribed to a degradation process, but rather to a more effective assembling of **3** in the PMMA matrix which slows down the rearrangement process leading to the reorientation of the chromophores within the polymeric matrix.

Conclusions

Novel nickel heteroleptic Donor-Acceptor complexes were prepared and their second-order NLO properties were investigated both in solution and in the bulk. The electronic properties of these D-A complexes were strongly influenced by the nature of the D and A ligands. In the present study, the A ligand (dithione moiety) was invariant, whereas the D ligand was modified by decreasing the electron withdrawing properties of the substituents attached to the dithiolate system on going from **1** to **4**. Moreover, in these ternary D-Ni-A complexes, D mainly contributed to the LUMO, whereas A dominated the HOMO, with the metal acting as an electronic bridge between D and A. Consequently, the HOMO-LUMO

energy gap decreased from **1** to **4**, according to the HOMO destabilization (see Figure 6). More importantly, since the optical properties mainly depend on the HOMO-LUMO gap, we could achieve a modulation of the low-energy absorption (see Figure 3). Compound **1**-**4** exhibited a relatively similar thermolytic behaviour, having decomposition temperatures above 200 deg. Nevertheless, when **1**-**4** were processed as thin films embedded into a PMMA poled matrix, only compound **3** maintained second order NLO properties at the solid state. A good NLO response was found with a value of the three nonzero coefficients of the second-order susceptibility tensor $\chi_{33}^{(2)}$, $\chi_{31}^{(2)}$, and $\chi_{15}^{(2)}$ = 2.20 ± 0.44 pm V^{-1}, 0.56 ± 0.12 pm V^{-1} and 0.42 ± 0.08 pm V^{-1}, respectively. It can be speculated that the presence of ester groups attached to the dithiolate moiety in **3** allowed a suitable assembly in the polymer film to achieve a stable and good SHG response in the bulk. The ester group were present also in **4**, but they are connected to the dithiolate system by a bent hexa-atomic ring, which may confer a more conformational mobility to **4** once incorporated into the matrix. The use of different polymeric matrices as polystyrene and polycarbonate having Tg below 200°C, or of a cross-linked polymeric network carrying covalently attached NLO chromophores, as well as introducing chiral substituents in the periphery of the molecule can be alternative strategies to achieve or improve the SHG response in the solid state.[54] These results, coupled with the high earth abundance and low cost production of nickel derivatives, make **3** an appealing 2nd NLO candidate to be processed for further development as optical material with SHG properties.[1-3]

Conflicts of interest

There are no conflicts to declare.

Acknowledgements

This research was supported by Università di Cagliari. The authors thank *Fondazione Banco di Sardegna* (Progetti Biennali di Ateneo–Annualità 2017. CUP:F71I17000170002). Regione Lombardia and Fondazione Cariplo are gratefully acknowledged for the use of instrumentation purchased through the SmartMatLab Centre project (2014).

Notes and references

1 J. Zyss, Molecular Nonlinear Optics: Materials, Physics and Devices; Academic Press: Boston, 1994.
2 M. G. Papadopoulos, J. Leszczynski and A. Sadlej, Nonlinear Optical Properties of Matter: From Molecules to Condensed Phases, ed. Springer, Dordrecht, 2006.
3 B. J. Coe, *In Non-Linear Optical Properties of Matter; Papadopoulos*, ed.s M. G., Sadlej, A. J., Leszczynski, Springer Verlag: Berlin, 2006, 571.
4 V. Guerchais, L. Ordronneau and H. Le Bozec, *Coord. Chem. Rev.* 2010, **254 (21-22)**, 2533−2545.
5 S. Di Bella, C. Dragonetti, M. Pizzotti, D. Roberto, F. Tessore, R. Ugo, in *Topics in Organometallic Chemistry 28, Molecular Organometallic Materials for Optics*, ed.s H. Le Bozec, V. Guerchais, Springer: New York, 2010, 28, 1 −55.
6 D. Espa, L. Pilia, S. S. Attar, A. Serpe and P. Deplano, *Inorg. Chimica Acta*, 2018, **470**, 295-302;
7 S. D. Cummings and R. Eisenberg, E. I. Stiefel, in *Progress in Inorganic Chemistry*, ed. E. I. Stiefel, Wiley: Chichester, 2004, vol. 52, 315-367.
8 S. D. Cummings, L.-T. Cheng and R Eisenberg, *Chem. Mater.*, 1997, **9** , 440-450.
9 L. Pilia, M. Pizzotti, F. Tessore and N. Robertson, *Inorg. Chem.* 2014, **53**, 4517-4526.
10 K. Base, M. T. Tierney, A. Fort, J. Muller and M. W. Grinstaff, *Inorg. Chem.* 1999, **38 (2)**, 287-289.
11 L. Pilia, D. Marinotto, M. Pizzotti, F. Tessore, N. Robertson**,** *J. Phys. Chem. C*, 2016, **120**, 19286–19294.
12 D. Espa, L. Pilia, L. Marchio, M. L. Mercuri, A. Serpe, A. Barsella, A. Fort, S. J. Dalgleish, N. Robertson and P. Deplano, *Inorg. Chem.* 2011, **50 (6)**, 2058–2060.
13 S. S. Attar, D. Espa, F. Artizzu, L. Pilia, A. Serpe, M. Pizzotti, G. Di Carlo, L. Marchiò and P. Deplano, *Inorg. Chem.*, 2017, **56**, 6763−6767.
14 D. Espa, L. Pilia, L. Marchiò, F. Artizzu, G. Di Carlo, D. Marinotto, A. Serpe, F. Tessore and P. Deplano, *Dalton Trans.*, 2016, **45**, 17431-17438.
15 L. Pilia, D. Espa, A. Barsella, A. Fort, C. Makedonas, L. Marchiò, M. L. Mercuri, A. Serpe, C. A. Mitsopoulou and P. Deplano, *Inorg. Chem.*, 2011, **50**, 10015-10027.
16 S.-G. Liu, Y.-Q. Liu, Y.-F. Li and D.-B Zhu, *Synth. Met.,* 1996, **83**, 131-140.
17 D. Eggerding and R. West, *J. Org. Chem.*, 1976, **41 (24)**, 3904–3909.
18 R. P. Parg, J. D. Kilburn, M. C. Petty, C. Pearson and T. G. Ryan, *Synthesis*, 1994, 613-618.
19 X. Yang, T. B. Rauchfuss and S. R. Wilson, *J. Chem. Soc., Chem. Commun.,* 1990, 34-36.
20 R. G. Parr and W. Yang, *Density-Functional Theory of Atoms and Molecules*; Oxford University Press: New York, 1989, 2010.
21 Gaussian 16, Revision B.01, M. J. Frisch, G. W. Trucks, H. B. Schlegel, G. E. Scuseria, M. A. Robb, J. R. Cheeseman, G. Scalmani, V. Barone, G. A. Petersson, H. Nakatsuji, X. Li, M. Caricato, A. V. Marenich, J. Bloino, B. G. Janesko, R. Gomperts, B. Mennucci, H. P. Hratchian, J. V. Ortiz, A. F. Izmaylov, J. L. Sonnenberg, D. Williams-Young, F. Ding, F. Lipparini, F. Egidi, J. Goings, B. Peng, A. Petrone, T. Henderson, D. Ranasinghe, V. G. Zakrzewski, J. Gao, N. Rega, G. Zheng, W. Liang, M. Hada, M. Ehara, K. Toyota, R. Fukuda, J. Hasegawa, M. Ishida, T. Nakajima, Y. Honda, O. Kitao, H. Nakai, T. Vreven, K. Throssell, J. A. Jr. Montgomery, J. E. Peralta, F. Ogliaro, M. J. Bearpark, J. J. Heyd, E. N. Brothers, K. N. Kudin, V. N. Staroverov, T. A. Keith, R. Kobayashi, J. Normand, K. Raghavachari, A. P. Rendell, J. C. Burant, S. S. Iyengar, J. Tomasi, M. Cossi, J. M. Millam, M. Klene, C. Adamo, R. Cammi, J. W. Ochterski, R. L. Martin, K. Morokuma, O. Farkas, J. B. Foresman, D. J. Fox, Gaussian, Inc., Wallingford CT, 2016.
22 A. D. Becke, *Phys. Rev. A*, 1988, **38 (6)**, 3098-3100.
23 A. D. Becke, *J. Chem Phys.,* 1993, **98 (7)**, 5648-5652.
24 R. Ditchfield, W. J. Hehre and J. A. Pople, *J. Chem. Phys.,* 1971, **54**, 724.
25 V. A. Rassolov, M. A. Ratner, J. A. Pople, P. C. Redfern and L. A. Curtiss, *J. Comp. Chem.*, 2001, **22**, 976.
26 T. H. Jr. Dunning and P. J. Hay, in *Modern Theoretical Chemistry*, Ed. H. F. Schaefer III, Vol. 3, Plenum, New York, 1977, 1-28.
27 P. Fuentealba, H. Preuss, H. Stoll and L. v. Szentpály, *Chem. Phys. Lett.*, 1982, **89**, 418-22.

28 M. A. Thompson, ArgusLab 4.0.1; Planaria Software LLC: Seattle, WA, http://www.arguslab.com/arguslab.com/ArgusLab.html/.
29 S. I. Gorelsky, AOMix: Program for Molecular Orbital Analysis; version 6.87, University of Ottawa, 2013, http://www.sg-chem.net/.
30 S. I. Gorelsky and A. B. P. Lever, *J. Organomet. Chem*., 2001, **635**, 187-196.
31 SMART (control) and SAINT (integration) software for CCD systems, Bruker AXS, Madison, WI, USA, 1994.
32 Area-Detector Absorption Correction; Siemens Industrial Automation, Inc.: Madison, WI, 1996.
33 W. Kabsch, *Acta Cryst. D,* 2010, **66(2)**, 125–132.
34 G. M. Sheldrick, *Acta Cryst. A*, 2015, **71**, 3-8.
35 G. M. Sheldrick, *Acta Crystallographica Section C*, 2015, **71**, 3-8.
36 O. V. Dolomanov, L. J. Bourhis, R. J. Gildea, J. A. K. Howard and H. Puschmann, *J. Appl. Cryst.*, 2009, **42**, 339-341.
37 C. F. Macrae, I. J. Bruno, J. A. Chisholm, P. R. Edgington, P. McCabe, E. Pidcock, L. Rodriguez-Monge, R. Taylor, J. van de Streek and P. A. Wood, *J. Appl. Cryst.*, 2008, **41**, 466-470.
38 A. Willetts, J. E. Rice, D. M. Burland and D. P. Shelton, *J. Chem. Phys.* 1992, **97**, 7590-7599.
39 P. D. Maker, R. W. Terhune, M. Nisenoff and C. M. Savage, *Phys. Rev. Lett*., 1962, **8**, 21-22.
40 J. Jerphagnon and S. K. Kurtz, *J. Appl. Phys.*, 1970, **41**, 1667-1681.
41 W. N. Herman and L. M. Hayden, *J. Opt. Soc. Am. B*, 1995, **12**, 416-427.
42 A. Obanda, K. Martinez, R. H. Schmehl, J. T. Mague, I. V. Rubtsov, S. N. MacMillan, K. M. Lancaster, S. Sproules, J. P. Donahue, *Inorg. Chem.*, 2017, **56 (17)**, 10257–10267.
43 S. C. Ratvasky, B. Mogesa, M. J. van Stipdonk and P. A. Basu; *Polyhedron*, 2016, **114**, 370-37.
44 D. Espa, L. Pilia, L. Marchiò, F. Artizzu, A. Serpe, M. L. Mercuri, D. Simão, M. Almeida, M. Pizzotti, F. Tessore and P. Deplano, *Dalton Trans.*, 2012, **41**, 3485-3493.
45 L. Pilia, F. Artizzu, C. Faulmann, M. L. Mercuri, A. Serpe and P. Deplano, *Inorg. Chem. Commun.*, 2009, **12**, 490-493.
46 C.-T. Chen, S.-Y. Liao, K.-J. Lin and L.-L. Lai, *Adv. Mater.*, 1998, **3,** 334-338.
47 S. S. Attar, F. Artizzu, L. Marchiò, D. Espa, L. Pilia, M. F. Casula, A. Serpe, M. Pizzotti, A. Orbelli-Biroli and P. Deplano, *Chem. Eur. J.*, 2018, **24**, 10503–10512.
48 C. R. Moylan, R. J. Twieg, V. Y. Lee, S. A. Swanson, K. M. Betterton and R. D. Miller, *J Am. Chem Soc.*, 1993, **115**, 12599-12600.M.
49 C. Downer, B. S. Mendoza and V. I. *Surf. Interface Anal.*, 2001, **31**, 966-986.
50 M. Makowska-Janusik, H. Reis, M. G. Papadopoulos, I. G. Economou and N. Zacharopoulos, *J. Phys. Chem. B*, 2004, **108**, 588–596.
51 R. H. Page, M. C. Jurich, B. Beck, A. Sen, R. J. Twieg, J. D. Swalen, G. C. Bjorklund, C. G. Wilson, *J. Opt. Soc. Am. B*, 1990, **7**, 1239−1250.
52 M. A. Mortazavi, A. Knoesen, S. T. Kowel, B. G. Higgins and A. Dienes, *J. Opt. Soc. Am. B*, 1989, **6**, 733−741.
53 A. Avramopoulos, H. Reis, N. Otero, P. Karamanis, C. Pouchan and M. G. Papadopoulos, *J. Phys. Chem. C*, 2016, **120 (17)**, 9419–9435.
54 D. Marinotto, S.Proutiere, C. Dragonetti, A. Colombo, P. Ferruti, D. Pedron, M.C. Ubaldi, S. Pietralunga, *J. of Non-Crystalline Solids*, 2011, **357**, 2075–2080.